NUMERICAL INVESTIGATION OF INSTABILITY OF AN ANNULAR ROTATING CAVITY

EWA TULISZKA-SZNITKO, ARTUR ZIELIŃSKI
AND JAROSŁAW POLUS

Chair of Thermal Engineering, Poznan University of Technology,
Piotrowo 3, 60-965 Poznan, Poland
sznitko@sol.put.poznan.pl

Abstract: A direct two-dimensional numerical simulation has been performed to study the transition flow in an annual rotating cavity. The spectral collocation method based on the Chebyshev polynomial is used to solve the incompressible Navier-Stokes equation. The time scheme is semi-implicit and second-order accurate; it corresponds to a combination of the second-order backward differentiation formula for the viscous diffusion term and the Adams-Bashforth scheme for the non-linear terms. The method uses a projection scheme to maintain the incompressibility constrain. The numerical computations, performed for an annular cavity of the aspect ratio $L = 2$ and 5 and for the curvature parameters $R_m = (R_1 + R_0)/(R_1 - R_0) = 5$, exhibit instability structures in the form of circular rolls. These structures are in good agreement with the other investigations, both experimental and theoretical.

Keywords: rotating cavity, direct method, laminar-turbulent transition

1. Introduction

Flows in rotating disk systems are not only a subject of fundamental interest but also a topic of practical importance. Typical configurations are cavities between the compressors and turbines disks. Numerous works have recently been devoted to the investigation of instabilities associated with a single disk flow (Kobayashi [1], Lingwood [2–4]) and differentially rotating disks' flow (Daube [5], Itoh [6], Tuliszka-Sznitko [7, 8], Serre [9–11], Cousin-Rittemard [12, 13]). In the case of the rotor/stator flows at high rotation rates, the flow consists of two boundary layers, *e.g.* of the Ekman type on the rotating disk and of the Bödewadt type on the stationary disk, separated by an inviscid rotating core. The transition process in both boundary layers is related to type I and type II generic linear instabilities. A type I instability is due to the presence of an inflection point in the boundary layer's velocity profile. The mechanism of type II instabilities is related to the combined effects of the Coriolis and viscous forces. Faller [14] and Caldwell [15] have investigated experimentally type I and type II

instabilities in the Ekman flow and found reasonably good agreement with the linear stability theory. Savas [16] has studied experimentally unsteady, uniformly rotating flow over a stationary disk and found both rings and spiral structures recognised as type II and type I instabilities, respectively. In both the rotor/stator cavity flow and the flows around a single disk, the experimental results exhibit similar instability structures; however, the confinement of the (rotor/stator) geometry has an effect on the critical Reynolds number.

Lingwood [2, 3] showed in her theoretical and experimental studies that the flow around a single rotating disk is absolutely unstable. Lingwood [4] also demonstrated theoretically that a rotating flow over a stationary disk is absolutely unstable. The recent theoretical (Tuliszka-Sznitko [7, 8]) and experimental (Gauthier [17]) research has revealed absolute instability in the rotor/stator flow.

The flow between two disks rotating in the rotor/stator configuration has been analysed with the assumption that the radius of the disks is either infinite (Itoh [6], Tuliszka-Sznitko [7, 8]) or finite (Daube [5], Serre [9–11], Cousin-Rittemard [12]). In the case of a finite radius of the disks, additional parameters are needed to describe the geometrical configuration and the imposed boundary conditions. Modifications introduced by the presence of external and internal shrouds and the influence of the attachment of the shrouds to the rotor or the stator have been discussed in many papers (Dijkstra [18], Adams [19], Cousin-Rittemard [12, 13], Oliveira [20]). Great influence of the end-walls boundary layers on the flow structure has been reported.

In the present paper we present our preliminary axisymmetric calculations for an annular geometry of the aspect ratio $L = 5$ and 2 and for the curvature parameter $R_m = 5$. This 2D assumption was principally dictated by computing requirements. The validity of the 2D assumption is questionable. Many of the experimental and numerical stability studies of the flow around rotating disks have shown that 3D spiral vortices are dominant. However, the experimental study performed by Savas [16] has proven the existence of cylindrical waves in the Bödewadt flow. The stability analysis of the similarity basic state performed by Itoh [6] and Tuliszka-Sznitko [7] has shown that the stationary disk boundary layer is far more unstable than the rotating one and that modes which propagate almost radially are the most unstable. Recent experimental works by Gauthier [17] and Schouveiler [21] have demonstrated that for small radial ratios R_1/R_0 cylindrical vortices can be found in the early transition stage. We treat the 2D calculations as a preliminary stage for further 3D calculations. At the same time we emphasise that the 2D calculations are not unphysical.

The paper is organized as follows. The geometrical and mathematical models are described in Sections 2 and 3, respectively, while the numerical technique is discussed in Section 4. The results are presented in Section 5 and the concluding remarks are given in Section 6.

2. The geometrical model

The geometrical model is a rotor-stator annular cavity of the aspect ratio $L = (R_1 - R_0)/2h = 2$ and 5 and the curvature parameter $R_m = \frac{(R_1 + R_0)}{(R_1 - R_0)} = 5$. The disks are bounded by stationary cylinders of height $2h$ (Figure 1).
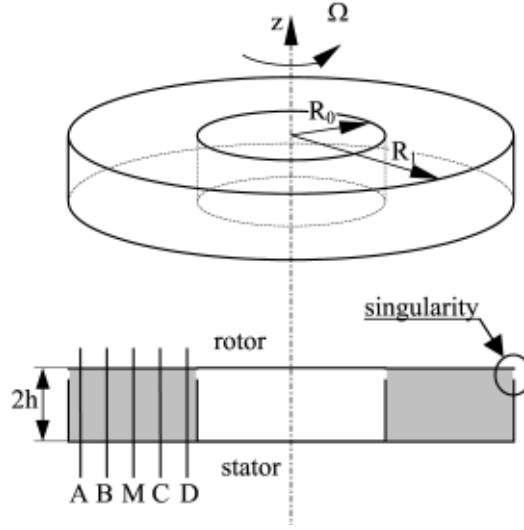
Figure 1. Schematic picture of the annular rotating cavity
with monitoring points in radial direction

The rotor rotates with uniform angular velocity $\Omega = \Omega e_z$, e_z being the unit vector. The origin of the z-axis is located at the mid-height between the disks. The governing parameters are the Reynolds number based on the external radius of the disks, $\mathrm{Re}_R = R_1^2 \Omega/\hat{v}$, the Reynolds number based on the height of the cylinder, $\mathrm{Re} = (2h)^2 \Omega/\hat{v}$, and the local Reynolds number based on the viscous scale $\delta = \sqrt{\hat{v}/\Omega}$, $\mathrm{Re}_\delta = \delta r^* \Omega/\hat{v} = \sqrt{r^{*2}\Omega/\hat{v}}$ (the asterisk denotes the dimensional value, and $\hat{v}$ denotes kinematic viscosity). The $\mathrm{Re}_R = R_1^2 \Omega/\hat{v}$ Reynolds number is the upper bound to the square of the local Reynolds number, $\mathrm{Re}_\delta = \sqrt{r^{*2}\Omega/\hat{v}}$. The local Reynolds number is used to discuss the instability thresholds and characteristic parameters of the instability waves.

3. The mathematical model

The governing equations are the 3D Navier-Stokes equations written in the velocity-pressure formulation together with the continuity equation. The equations are written in a cylindrical polar coordinate system (r, z, φ), with respect to a stationary frame of reference:

$$\frac{\partial V}{\partial t} = \frac{1}{\mathrm{Re}}\Delta V - (V \cdot \nabla)V - \nabla P, \qquad \nabla \cdot V = 0, \tag{1}$$

where t is time, V is the velocity vector, (u, w, v) are the velocity components in the r, z, and φ directions, respectively, and P is pressure. The scales for the dimensionless variables of time and velocity are Ω^{-1} and ΩR_1, respectively. The dimensionless axial co-ordinate is $z = z^*/h$; $z \in [-1,1]$. The radius co-ordinate is normalized to obtain the $[-1,1]$ domain required by the spectral method based on the Chebyshev polynomials: $r = (2r^* - (R_1 + R_0))/(R_1 - R_0)$. The boundary conditions are as follows: no slip boundary conditions at all rigid walls $u = w = 0$. For the azimuthal velocity component the boundary conditions are $v = 0$ on the stator and $v = (R_m + r)/(R_m + 1)$ on the rotating disk. The azimutal velocity on the stationary end-walls is equal to zero,

$v = 0.0$. However, this boundary condition must be modified because of the singularity of the azimuthal velocity at the junction between the stationary end-walls and the rotating disk. The singularity expresses a physical situation where there is a thin gap between the edge of the rotating disk and the stationary end-walls. To eliminate the singularity, different azimuthal velocity profiles are used for $r = \pm 1$: the linear profile $v = (1 + z)(R_m + r)/2(R_m + 1)$ (Serre and Pulicani [10]) and the exponential profile $v = \exp((z - 1)/0.006)$ (Serre, Tuliszka-Sznitko and Bontoux [11]).

The computations start with a Reynolds number low enough to obtain stable flow, *e.g.* $\mathrm{Re}_R = R_1^2 \Omega / \hat{v} = 3000$. This solution is then used as an initial condition for a computation for a higher Reynolds number. For the first iteration we use as the initial condition the flow which corresponds to no motion in the meridional plane and to the linear azimutal velocity profile: $u = 0$, $v = (1 + r)(z + 1)/4$, $w = 0$.

4. Direct numerical simulation (DNS)

In this paper we restrict ourselves to a 2D flow. The numerical solution is based on a spectral collocation method (Canuto [22]). The Gauss-Lobatto collocation points are used:

$$r_i = \cos(i\pi/N), \quad z_j = \cos(j\pi/M), \quad i = 0, \ldots, N, \quad j = 0, \ldots, M,$$
$$(r_i, r_j) \in [-1, 1] \times [-1, 1], \tag{2}$$

where N and M are the number of collocation points in the radial and axial directions, respectively. The $\Psi = (u, w, v, P)$ solution of Equations (1) is approximated by means of a Chebyshev polynomial expansion in the r and z directions (Serre [9, 10]):

$$\Psi(r, z, t) = \sum_{n=0}^{N} \sum_{m=0}^{M} \hat{\Psi}_{nm} T_n(r) T_m(z) \quad \text{for} \quad -1 \le r, z \le 1, \tag{3}$$

where $\hat{\Psi}_{nm}$ are the spectral coefficients, while T_n and T_m are Chebyshev polynomials. The time scheme is semi-implicit and second-order accurate. It corresponds to a combination of the second-order backward differentiation formula for the viscous diffusion term and the Adams-Bashforth scheme for the non-linear terms. The method uses a projection scheme to maintain the incompressibility constrain. Details are described in [10].

We transform Equations (1) into a more convenient form (Serre [9, 10]):

$$\frac{1}{L}\frac{\partial u}{\partial r} + \frac{u}{L(R_m + r)} + \frac{\partial w}{\partial z} = 0, \tag{4}$$

$$\frac{\partial u}{\partial t} + L(R_m + 1)Au = -(R_m + 1)\frac{\partial P}{\partial r} + \frac{L^2(R_m + 1)^2}{\mathrm{Re}_R}\left[\Delta u - \frac{u}{L^2(R_m + r)^2}\right], \tag{5}$$

$$\frac{\partial v}{\partial t} + L(R_m + 1)Av = \frac{L^2(R_m + 1)^2}{\mathrm{Re}_R}\left[\Delta v - \frac{v}{L^2(R_m + r)^2}\right], \tag{6}$$

$$\frac{\partial w}{\partial t} + L(R_m + 1)Aw = -L(R_m + 1)\frac{\partial P}{\partial z} + \frac{L^2(R_m + 1)^2}{\mathrm{Re}_R}[\Delta w], \tag{7}$$

where

$$Au = \frac{1}{L}u\frac{\partial u}{\partial r} + w\frac{\partial u}{\partial z} - \frac{v^2}{L(R_m + r)}, \qquad Av = \frac{1}{L}u\frac{\partial v}{\partial r} + w\frac{\partial v}{\partial z} + \frac{uv}{L(R_m + r)},$$
$$Aw = \frac{1}{L}u\frac{\partial w}{\partial r} + w\frac{\partial w}{\partial z}. \tag{8}$$

The cylindrical Laplacian operator for the two-dimensional flow is defined in the following way:

$$\Delta = \frac{1}{L^2}\frac{\partial^2}{\partial r^2} + \frac{1}{L^2(R_m+r)}\frac{\partial}{\partial r} + \frac{\partial^2}{\partial z^2}. \tag{9}$$

4.1. Predictor

The first task is to obtain pressure distribution. The pressure predictor, P^p, is computed from the so-called pressure elliptic equation derived from the continuity Equation (4) and Navier-Stokes Equations (5)–(7):

$$\Delta P^p = -\mathrm{divergence}(N(V)), \tag{10a}$$

where $N(V)$ denotes the non-linear terms of the Navier-Stokes equations, $N(V) = [(N(V))_r, (N(V))_\varphi, (N(V))_z]^T$. For numerical purposes and the 2D flow, we write this equation in the following manner:

$$\frac{1}{L^2}\frac{\partial^2 P^p}{\partial r^2} + \frac{1}{L^2(R_m+r)}\frac{\partial P^p}{\partial r} + \frac{\partial^2 P^p}{\partial z^2} = -2\left[\frac{1}{L}\frac{\partial}{\partial r}Au^n + \frac{1}{L}\frac{1}{R_m+r}Au^n + \frac{\partial}{\partial z}Av^n\right] +$$
$$+ \left[\frac{1}{L}\frac{\partial}{\partial r}Au^{n-1} + \frac{1}{L}\frac{1}{R_m+r}Au^{n-1} + \frac{\partial}{\partial z}Av^{n-1}\right]. \tag{10}$$

Equation (10) is solved with the following boundary conditions:

$$\frac{\partial P^p}{\partial r} = -L\left[(2Au^n - Au^{n-1})\right] +$$
$$+ \frac{L^2(R_m+1)}{\mathrm{Re}_R}\left[2\left(\Delta u^n - \frac{u^n}{L^2(R_m+r)^2}\right) - \left(\Delta u^{n-1} - \frac{u^{n-1}}{L^2(R_m+r)^2}\right)\right],$$
$$\frac{\partial P^p}{\partial z} = -\left[(2Aw^n - Aw^{n-1})\right] + \tag{11}$$
$$+ \frac{L(R_m+1)}{\mathrm{Re}_R}\left[2\left(\Delta w^n - \frac{w^n}{L^2(R_m+r)^2}\right) - \left(\Delta w^{n-1} - \frac{w^{n-1}}{L^2(R_m+r)^2}\right)\right].$$

The velocity predictor is calculated from the following equations:

$$\Delta u^p - u^p\frac{1}{L^2(R_m+r)^2} - \frac{\mathrm{Re}_R}{L^2(R_m+1)^2}\frac{3}{2}\frac{u^p}{\delta t} =$$
$$\frac{\mathrm{Re}_R}{L^2(R_m+1)^2}\left(\frac{-4u^n+u^{n-1}}{2(\delta t)} + L(R_m+1)(2Au^n - Au^{n-1}) + (R_m+1)\frac{\partial P^p}{\partial r}\right),$$
$$\Delta v^p - v^p\frac{1}{L^2(R_m+r)^2} - \frac{\mathrm{Re}_R}{L^2(R_m+1)^2}\frac{3}{2}\frac{v^p}{\delta t} =$$
$$\frac{\mathrm{Re}_R}{L^2(R_m+1)^2}\left(\frac{-4v^n+v^{n-1}}{2(\delta t)} + L(R_m+1)(2Av^n - Av^{n-1})\right), \tag{12}$$
$$\Delta w^p - \frac{\mathrm{Re}_R}{L^2(R_m+1)^2}\frac{3}{2}\frac{w^p}{\delta t} =$$
$$\frac{\mathrm{Re}_R}{L^2(R_m+1)^2}\left(\frac{-4w^n+w^{n-1}}{2(\delta t)} + L(R_m+1)(2Aw^n - Aw^{n-1}) + L(R_m+1)\frac{\partial P^p}{\partial z}\right).$$

The boundary conditions for the above equations are as follows:

$$u^p = u^{n-1}, \qquad v^p = v^{n-1}, \qquad w^p = w^{n-1}. \tag{13}$$

4.2. Corrector

Corrections of pressure and velocity are calculated from the following equations:

$$\frac{3}{2(\delta t)}(u^{n+1} - u^p) = -(R_m+1)\left(\frac{\partial P^{n+1}}{\partial r} - \frac{\partial P^p}{\partial r}\right),$$

$$\frac{3}{2(\delta t)}(v^{n+1} - v^p) = 0, \tag{14}$$

$$\frac{3}{2(\delta t)}(w^{n+1} - w^p) = -(R_m+1)L\left(\frac{\partial P^{n+1}}{\partial z} - \frac{\partial P^p}{\partial z}\right),$$

and

$$\frac{1}{L}\frac{\partial u^{n+1}}{\partial r} + \frac{u^{n+1}}{L(R_m+r)} + \frac{\partial w^{n+1}}{\partial z} = 0. \tag{15}$$

The boundary conditions for Equations (15) are:

$$V^{n+1} \cdot n = V^p \cdot n. \tag{16}$$

We calculate u^{n+1}, v^{n+1}, w^{n+1}, p^{n+1} by introducing a new value,

$$\phi = 2\delta t(P^{n+1} - P^p)/3, \tag{17}$$

to Equations (14)–(15). Finally, we obtain:

$$\frac{1}{L^2}\frac{\partial^2 \phi}{\partial r^2} + \frac{1}{L^2(R_m+r)} \cdot \frac{\partial \phi}{\partial r} + \frac{\partial^2 \phi}{\partial z^2} =$$
$$\frac{1}{L(R_m+1)}\left(\frac{1}{L}\frac{\partial u^p}{\partial r} + \frac{u^p}{L(R_m+r)} + \frac{\partial w^p}{\partial z}\right). \tag{18}$$

The boundary condition for this equation is:

$$\mathrm{grad}(\phi) \cdot n = 0. \tag{19}$$

The corrected pressure and velocity are as follows:

$$P^{n+1} = P^p + \frac{3}{2\partial t}\phi, \qquad V^{n+1} = V^p - \mathrm{grad}(\phi). \tag{20}$$

At every new time level $(n+1)\delta t$ each flow variable $\Psi(u^p, v^p, w^p, p^p, \phi)$ is the solution of a 2D equation of the following form (Serre [10]):

$$\frac{1}{L^2}\frac{\partial^2 \Psi}{\partial r^2} + \frac{1}{L^2(R_m+r)}\frac{\partial \Psi}{\partial r} + \frac{\partial^2 \Psi}{\partial z^2} - \lambda\Psi = S, \tag{21}$$

where λ is a constant. The above equation is approximated by the spectral collocation method and the right-hand side of the Equation (21) is evaluated by a standard spectral technique. Then, full diagonalization is used to solve Equation (21) (Haldenwang [23]). For an annular cavity, the matrices of the radial and axial operators are diagonalizable with real eigenvalues. Details of the technique can be found in Serre and Pulicani [10] and Haldenwang [23].

5. Results

Numerical investigations have been performed for a rotating annular cavity of aspect ratio $L = 2$ and 5, for the curvature parameter $R_m = 5$. A linear profile for the azimutal velocity component was used to eliminate the singularity at the junctions between the stationary end-walls and the rotor, $v = (1+z)(R_m+r)/2(R_m+1)$. After some preliminary computations, a special resolution of 65×41 in the r and z directions, respectively, was chosen. However, we are aware that some additional grid tests are necessary, particularly in computations for higher Re_R planned for future publications. The incorporated time step was equal to $5 \cdot 10^{-3}$. The velocity fluctuations were computed with respect to the average flow solution.

Computations started with a Reynolds number low enough to obtain the steady flow, *e.g.* $\mathrm{Re}_R = R_1^2 \Omega / \hat{v} = 3000$. The criterion assumed for the steady flow was as follows:

$$|V^{n+1} - V^n|/\delta t \leq 10^{-5}. \tag{22}$$

The rotation of the rotor was then increased step by step with a very small increment equal to $\Delta \mathrm{Re}_R = 500$. The behaviour of the dependent variables was monitored at 15 points in five different positions in the radial direction $N(1/6, 1/3, 1/2, 2/3, 5/6)$ and in three positions in the axial direction $M(9/10, 1/2, 1/10)$, where N and M are numbers of collocation points in the radial and axial direction, respectively. The monitoring points in the radial direction are marked by letters A, B, M, C and D in Figure 1.

Preliminary results obtained for $L = 2$ and 5 and $R_m = 5$ are presented below. Let us first consider the results obtained for the aspect ratio $L = 2$.

The base flow was steady and composed of two disjoint boundary layers (one on each disk) and a central core flow. A fluid was pumped radially outwards along the rotating disk and radially inwards over the stationary disk. Both boundary layers were separated by the core rotating with near solid rotation.

In Figures 2a and 2b the time histories are presented of the axial velocity component obtained for $\mathrm{Re}_R = 32\,000$ and $34\,000$, respectively, at monitoring point M in the stationary and rotating disk boundary layers. Having examined the time history obtained for $\mathrm{Re}_R = 32\,000$, we can see that the first disturbances, introduced by the change of the Reynolds number, were dampened and the flow finally reached a steady state. For the higher Reynolds number, $\mathrm{Re}_R = 34\,000$, the first disturbances were dampened as well but then disturbances began to grow. We recognised the Reynolds number of $34\,000$ as the critical Reynolds number of the first bifurcation for the case of $R_m = 5$ and $L = 2$. This solution is fully oscillatory, as noticeable in Figure 2c, where part of the time history of this case is presented. From Figure 2c we can calculate the angular frequency $\sigma = 2\pi/\Delta t \sim 3.11$. For this Reynolds number, the amplitudes of disturbances in both boundary layers are small, but they grow quickly with the increasing Reynolds number. Their maximum occurs at the monitoring point D. We have observed the same angular frequency of disturbances at all monitoring points.

The disturbances' structure obtained for $\mathrm{Re} = 34\,000$ and $t = 250$ is presented in Figure 3, where the iso-lines of the azimuthal velocity component disturbances are

shown. In the stationary disk's boundary layer we can observe four pairs of counter-rotating vortices of the average wave length about $\lambda^*/h = 0.85$ or $\lambda^*/\delta = 13$, which propagate radially inwards with the average phase speed of $V_\phi/\Omega r = (\lambda_r^*/\delta)/\Delta t \mathrm{Re}_\delta = -0.042$ (the minus sign shows the direction of propagation). In the rotating disk's boundary layer we can observe three pairs of spiral vortices propagating with the phase speed of 0.073 radially outwards, in accordance with direction of the base flow. The radial wavelength of disturbances is defined as $\lambda_r^* = \Delta r^*/n_r$, where Δr^* is the radial length occupied by n_r rolls.
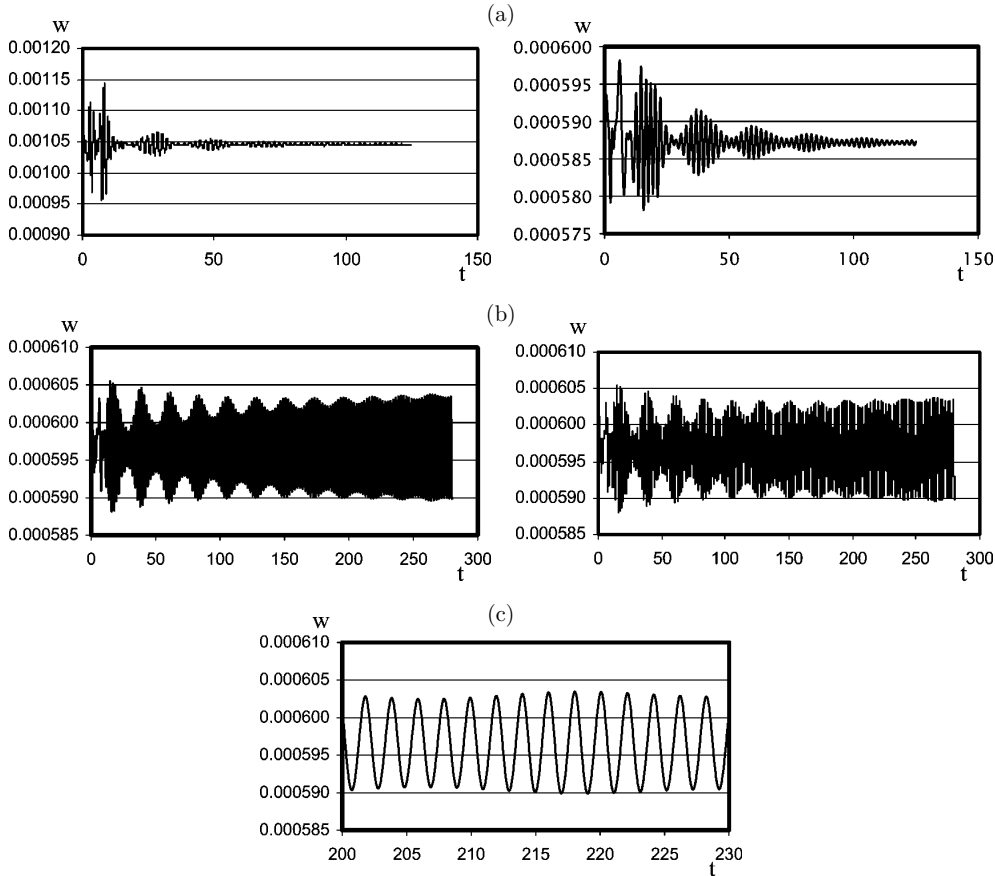
Figure 2. The time history of the axial velocity component obtained at monitoring point M of the stator and rotor boundary layers for (a) $\mathrm{Re}_R = 32\,000$ and (b) $34\,000$. (c) is a fragment of the time history presented in (b); $R_m = 5$ and $L = 2$

The time histories obtained for $L = 5$ and for $\mathrm{Re}_R = 69\,000$ and $72\,000$ in the stationary and rotating disk boundary layers are presented in Figures 4a and 4b, respectively. In both boundary layers we can observe the oscillatory solution of the angular frequency $\sigma = 2\pi/\Delta t = 4.5$. We determined the Reynolds number critical to unsteadiness to be $68\,500$. In Figure 5a, 5b and 5c the iso-lines of the azimuthal velocity component fluctuations obtained for $\mathrm{Re}_R = 69\,000$ at $t = 10$, 40 and 120 are presented, respectively.
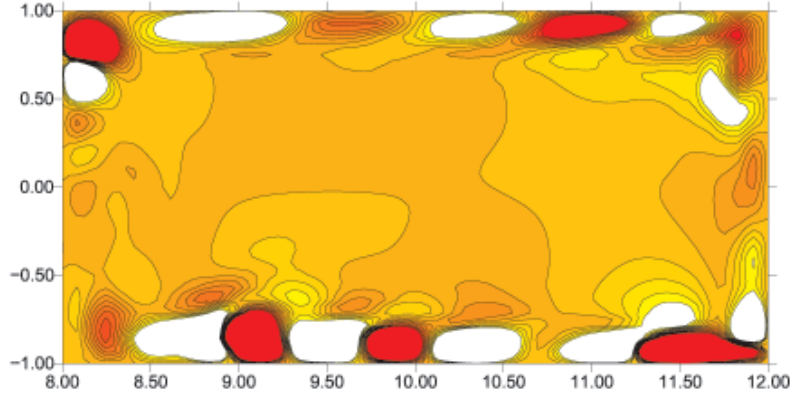
Figure 3. The iso-lines of disturbances of the azimuthal velocity component
in the $(r^*/h, z^*/h)$ plane; $\mathrm{Re}_R = 34\,000$, $R_m = 5$, $L = 2$ and $t = 250$
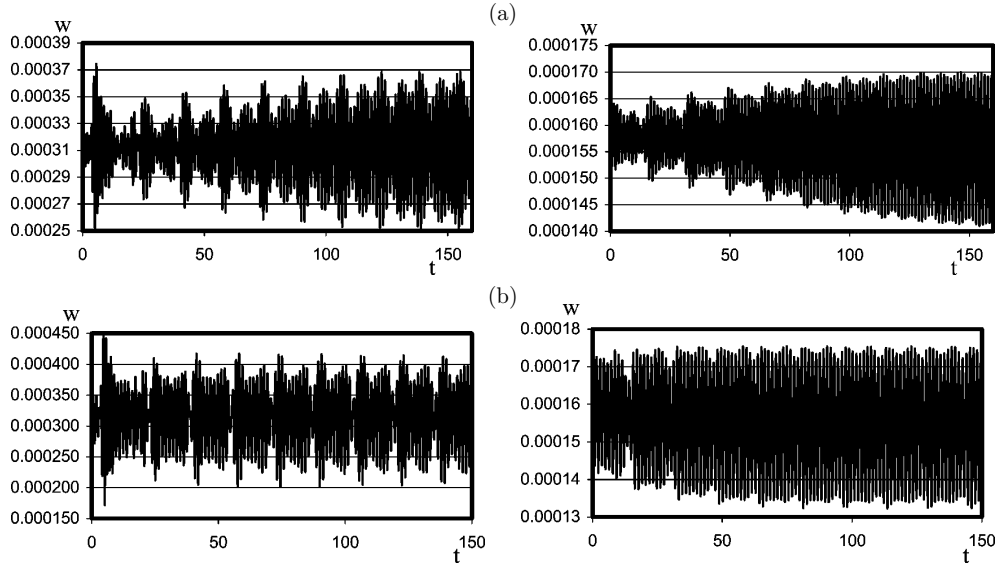
Figure 4. The time history of the axial velocity component obtained at monitoring point M of
the stator and rotor boundary layer obtained for
(a) $\mathrm{Re}_R = 69\,000$ and (b) $\mathrm{Re}_R = 72\,000$; $R_m = 5$ and $L = 5$

From Figure 5 we can see that stationary disk's boundary layer is less stable than that of the rotating disk (see also the time history). In the stationary disk's boundary layer we can observe four pairs of spiral vortices of wavelengths $8.7 < \lambda_r^*/\delta < 30$, which propagate radially inwards with the phase speed $-0.097 < V_\phi^*/\Omega r^* < -0.0338$. In the rotating disk's boundary layer we can observe two pairs of vortices, with $\lambda_r^*/\delta \sim 35$ and $V_\phi^*/\Omega r^* = 0.114$. We can see that structures obtained for $t = 40$ and 120 are very similar, whereas for $t = 10$ (the beginning of the time history, Figure 4a) the disturbances in the rotating disk's boundary layer are hardly visible. The iso-lines obtained for $\mathrm{Re}_R = 72\,000$ and $t = 120$ (Figure 6) are very similar to those obtained for $\mathrm{Re}_R = 69\,000$ (Figure 5c). The presented structures obtained for $L = 5$ have been compare with the 2D results obtained by Daube [5] (who has published

(a)

(b)

(c)
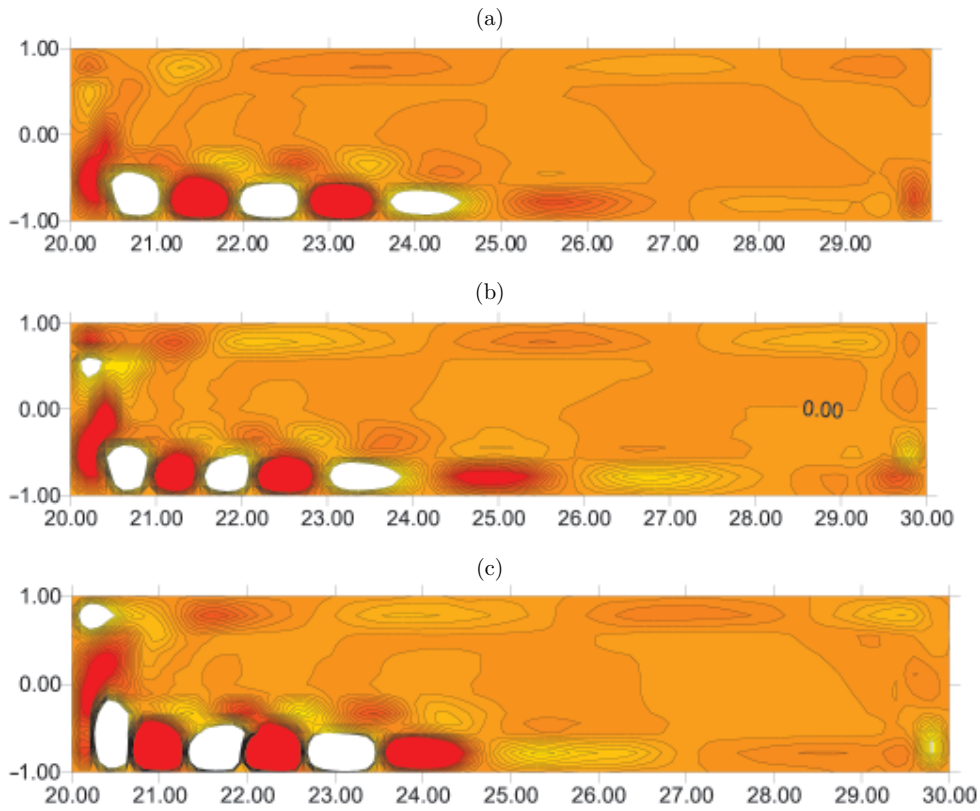
Figure 5. The iso-lines of disturbances of the azimuthal velocity component in the $(r^*/h, z^*/h)$ plane; (a) $t = 10$, (b) $t = 40$, (c) $t = 120$; $Re_R = 69\,000$, $R_m = 5$, $L = 5$
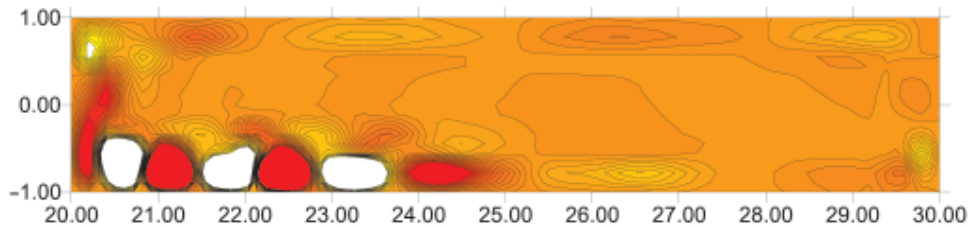
Figure 6. The iso-lines of disturbances of the azimuthal velocity component in the $(r^*/h, z^*/h)$ plane; $Re_R = 72\,000$, $R_m = 5$, $L = 5$ and $t = 120$

several results for $L = 5$ and various R_0/R_1 factors) and good qualitative agreement has been found.

6. Conclusions

The two-dimensional incompressible flow in the annular rotating cavity of the aspect ratio $L = 2$, 5 and $R_m = 5$ has been investigated numerically using a direct numerical simulation based on the spectral collocation method. We focused our attention on the first bifurcation to unsteadiness. The study of the first stages of the transition to turbulence, using as highly accurate DNS as here, is valuable as it allows for an accurate description of the instability mechanisms which are known to

play an important role in the process of breakdown to turbulence. We have presented the instability structures occurring in the stationary and rotating disks' boundary layers and the critical Reynolds numbers of the transition to unsteadiness have been given. The presented structures are in good qualitative agreement with the 2D results of Daube [5]. For both of the analyzed cases, $L = 2$ and $L = 5$, we have obtained an oscillatory solution.

Acknowledgements

References

[1] Kobayashi R, Kohama Y and Takamadate Ch 1980 *Acta Mechanika* **35** 71
[2] Lingwood R 1995 *J. Fluid. Mech.* **299** 17
[3] Lingwood R 1996 *J. Fluid. Mech.* **314** 373
[4] Lingwood R 1997 *J. Fluid. Mech.* **331** 405
[5] Daube O, Le Quéré P, Cousin-Rittemard M and Jacques R 2001 *J. Fluid Mech.* (submitted)
[6] Itoh M 1991 *ASME FED* **114** 83
[7] Tuliszka-Sznitko E and Soong C-Y 2000 *Proc. European Congress on Computational Methods in Applied Sciences and Engineering*, Barcelona, Spain, CDROM
[8] Tuliszka-Sznitko E, Serre E and Bontoux P 2002 *C.R. Mecanique* **30** 90
[9] Serre E, Crespo del Arco and Bontoux P 2001 *J. Fluid. Mech.* **434** 65
[10] Serre E and Pulicani J 2001 *Computers and Fluids* **30** 491
[11] Serre E, Tuliszka-Sznitko E and Bontoux P 2004 *Phys. of Fluids* **16** (3) 688
[12] Cousin-Rittemard N 1996 *Contribution à l'étude des instabilités des écoulements axisymetriques en cavité inter-disque de type rotor-stator*, Doctorate Thesis, Université de Paris VI
[13] Cousin-Rittemard N, Daube O and Le Quéré P 1998 *C.R. Acad. Sci., serie IIb* **326** 359
[14] Faller A J 1963 *J. Fluid Mech.* **15** 560
[15] Caldwell D R and Van Atta C 1970 *J. Fluid Mech.* **44** 79
[16] Savas O 1987 *J. Fluid Mech.* **183** 77
[17] Gauthier G, Gondret P and Rabaud M 1999 *J. Fluid Mech.* **386** 105
[18] Dijkstra D and Heijst G 1983 *J. Fluid Mech.* **128** 123
[19] Adams M L and Szeri A 1982 *J. Appl. Mechanics* **49** 1
[20] Oliviera L A, Pecheux J and Restivo A O 1991 *Teoret. Comp. Fluid Dyn.* **2** 211
[21] Schouveiler L, Le Gal P, Chauve M P and Takeda Y 1999 *Experiments in Fluids* **26** 179
[22] Canuto C, Hussaini M Y, Qarteroni A and Zang T A 1988 *Spectral Methods in Fluids Dynamics*, Springer
[23] Haldenwang P, Labrosse G, Abboudi S and Deville M 1984 *J. Comput. Phys.* **55** 115